Electronic Supplementary Material (ESI) for Sustainable Energy & Fuels.

Solar cell contacts: Quantifying the impact of interfacial layers on selectivity, recombination, charge transfer, and V_{oc}

Supplementary Information

Kira E. Egelhofer Ruegger[a], Ellis T. Roe[b], Mark C. Lonergan[a*]

[a]Department of Chemistry and Biochemistry, The Materials Science Institute, University of Oregon, Eugene, Oregon 97403, United States

[b]Department of Physics, University of Oregon, Eugene, Oregon 97403, United States

[*]Corresponding Author: lonergan@uoregon.edu

Non-baseline-corrected *operando* measurements

Fig. S1 shows the same plots as Fig. 5 but with data that has not been corrected for the baseline effects of atmosphere. Both before and after the potential step is applied, there is a slight linear trend in all the data due to the effects of the nitrogen atmosphere on the films, which before measurement were in air for six hours then nitrogen for 90 minutes.

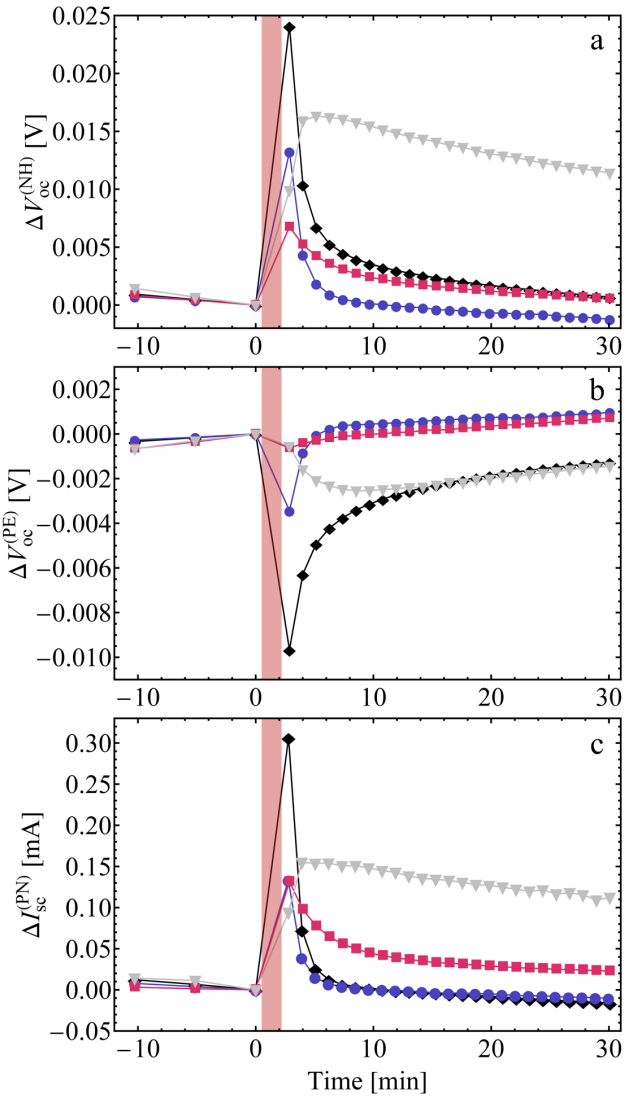

Fig S1 Non-baseline-corrected changes to $V_{oc}^{(PE)}$, $V_{oc}^{(NH)}$, and $I_{sc}^{(PN)}$ when potential steps are applied to the Li-TFSI-containing spiro-OMeTAD-modified gold contact when it acts as the hole contact (is measured *vs.* the n^+-Si back contact). Black diamonds indicate forward bias V_{app}, blue circles are $V_{app} = V_{oc}$, fuchsia squares are V_{app} = 0V, and gray inverted triangles are reverse bias V_{app}. The red shaded area indicates the time during which the voltage is applied under illumination.

Simulation details

The structure of the experimental IBC cell is as follows: IFL ~3-5 nm, top contact 50 nm, interdigitated contacts ~250 μm wide with same spacing, lightly doped n-Si bulk ~200 μm thick, doped silicon wells ~1 μm deep and ~500 μm wide). Unmodified IBC cells were generously donated by SunPower.

Numerical simulations were performed using the COMSOL 2D semiconductor module at 300K with a 2.25 mm wide and 200 μm thick silicon absorber (Fig. S2) with 0.392 cm cross section (for which measured values were corrected; direct current scaling was verified). The bulk silicon is lightly n-doped (10^{15} cm^{-3}) with n^+- and p^+-doped regions on the bottom (495 μm wide and 2 μm deep) with their respective ohmic metal contacts (250 μm wide in the middle of the dopant well). Beer-Lambert Generation was used in defined areas to account for contact "shadowing." Auger and SRH Recombination were present everywhere in the device. The top contact was simulated with a metal Schottky contact 2.25 mm wide on the top of the silicon bulk. To generate the simulation results, the program calculated $V_{oc}^{(PE)}$, $V_{oc}^{(NH)}$, and $I_{sc}^{(PN)}$ of the device with a normal mesh while varying J_{0p}/J_{0n} (from 2.3×10^{-7} to 1.4×10^{6}) and $(J_{0n}J_{0p})^{0.5}$ (from 3.5×10^{-8} to 3.5×10^{-3} A/cm^2) of the top metal contact. Shut resistance was introduced at the back side (in between the metal contacts) to match experimental V_{oc}s of pristine IBC cells. Table S1 shows the parameters used in the simulations.

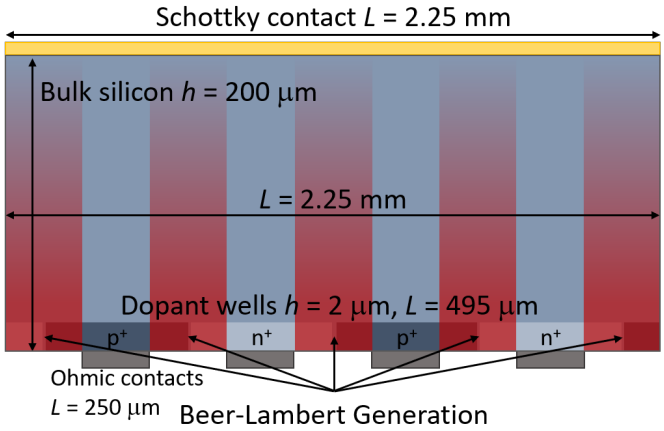

Fig S2 Two-dimensional IBC cell model used in COMSOL simulations.

Table S1 Simulation model parameters

Symbol	Description	Value
T	Temperature	300 K
E_g	Band gap	1.12 eV
ε_r	Relative permittivity	11.7
χ_0	Electron affinity	4.05 V
N_C	Effective conduction band DOS	10^{19} cm^{-3}
N_V	Effective valence band DOS	2.7×10^{19} cm^{-3}
$N_{D,b}$	Dopant density, bulk Si	10^{15} cm^{-3}
$N_{A,d}$	Dopant density, p^{+-}Si dopant wells	10^{18} cm^{-3}
$N_{D,d}$	Dopant density, n^{+}-Si dopant wells	10^{18} cm^{-3}
u_n	Electron mobility	1448 cm^{2}V^{-1}s^{-1}
u_p	Hole mobility	473 cm^{2}V^{-1}s^{-1}
G_L	Electron and hole Beer-Lambert generation rate; y is distance on y coordinate	$(1.52\times10^{21})\exp(-y/\alpha[\mu m^{-1}])$ cm^{-3}s^{-1}
α	Absorption depth	10 μm
res	Resistance between back p & n contacts	0 Ω for $I_{sc}^{(PN)}$, 10^{10} Ω for $V_{oc}^{(PE)}$ and $V_{oc}^{(NH)}$
J_{0p}/J_{0n}	Contact selectivity, top contact	2.3×10^{-7} to 1.4×10^{6} as a geometric series with common ratio 4.7
$(J_{0n}J_{0p})^{0.5}$	Interfacial recombination, top contact	3.5×10^{-8} to 3.5×10^{-3} A/cm^2 as a geometric series with common ratio 1.3
C	Auger recomb. coeff. for electrons and holes	2.0×10^{-30} cm^6/s
τ	SRH lifetime for electrons and holes	1 ms in bulk silicon; 10 μs in dopant wells

Details of extracting J_0 values from experiment and simulation

The data shown in Fig. S3 illustrate the relationship between simulated and experimentally measured $V_{oc}^{(PE)}$–$V_{oc}^{(NH)}$ and $I_{sc}^{(PN)}$ data and show the effects of air exposure and pre-measurement forward bias (0.8 V) on $V_{oc}^{(PE)}$–$V_{oc}^{(NH)}$ and $I_{sc}^{(PN)}$. To extract J_0 values from experimental $V_{oc}^{(PE)}$, $V_{oc}^{(NH)}$, and $I_{sc}^{(PN)}$ measurements, we generate an interpolation function relating simulated $V_{oc}^{(PE)}$–$V_{oc}^{(NH)}$ and $I_{sc}^{(PN)}$ values to the J_{0p}/J_{0n} and $(J_{0n}J_{0p})^{0.5}$ used to generate them. The interpolation function is solved using the experimental $V_{oc}^{(PE)}$–$V_{oc}^{(NH)}$ and $I_{sc}^{(PN)}$ data to find the corresponding J_{0p}/J_{0n} and $(J_{0n}J_{0p})^{0.5}$ values which are then used to calculate the individual J_{0n} and J_{0p}s. The same process is used with the QFLS simulation results to determine experimental QFLS values. The gold contact is treated slightly differently in the interpolation than filmed samples. Because it resides in the bulk recombination limit, we set the value of the Richardson Coefficient, A^*, to the value for metals. We only then use the interpolation function to determine the J_{0p}/J_{0n} and $(J_{0n}J_{0p})^{0.5}$ for unmodified gold. The values of $V_{oc}^{(PE)}$–$V_{oc}^{(NH)}$ and $I_{sc}^{(PN)}$ that correspond to the extracted J_{0p}/J_{0n} and $(J_{0n}J_{0p})^{0.5}$ for gold are shown as the red target in Fig. S3.

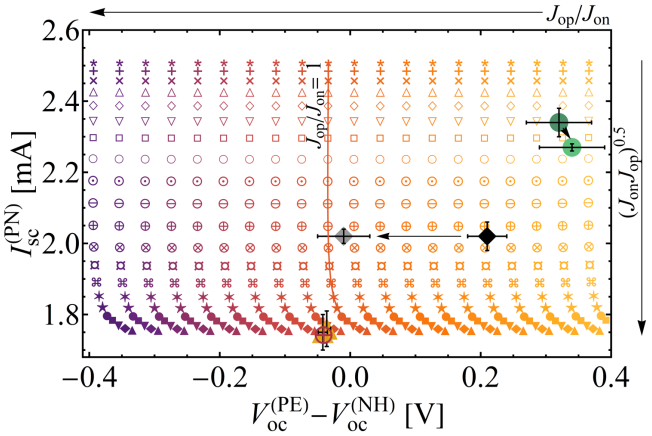

Fig S3 Simulation results for $V_{oc}^{(PE)}$-$V_{oc}^{(NH)}$ and $I_{sc}^{(PN)}$ as a function of J_{0p}/J_{0n} and $(J_{0n}J_{0p})^{0.5}$ with experimental data overlaid. Green circles are neat spiro-OMeTAD-modified gold, black and gray diamonds are Li-TFSI-containing spiro-OMeTAD-modified gold, and yellow triangles are unmodified gold. Arrows indicate direction of change upon exposure to air. For the simulated data, symbols indicate $(J_{0n}J_{0p})^{0.5}$ with values increasing from top to bottom as a geometric series from 3.5×10^{-8} to 3.5×10^{-6} A/cm^2 with common ratio 1.3. Data with the same values of J_{0p}/J_{0n} lie in quasi vertical groupings of the same color, for example as marked for the J_{0p}/J_{0n} = 1 data. The J_{0p}/J_{0n} increases from right to left as a geometric series from 1.5×10^{-7} (lightest orange) to 9.1×10^{5} (darkest purple) with common ratio 4.7.

Semiconductor contact boundary conditions

The boundary condition of equation 1 in the main text is widely used in the modelling of semiconductor interfaces. It is reproduced here:

$$J_{\mathrm{x}} = J_{0\mathrm{x}}\left(e^{\left(\frac{qV}{kT}\right)} - 1\right) \qquad S1$$

One simple view is that eqn (S1) is a phenomenological equation that treats each of the electron and hole as a partial current diode. The diode equation is typically applied to the total current at a very wide range of semiconductor interfaces, but it can also be applied to each of the carriers separately, leading to partial current diodes. When considered as such, the interface is modelled as two such diodes in parallel, one for electrons and one for holes, as previously reported by Rau and Kirchartz.[1] Hence, our interpretation and treatment in terms of J_0 values extracted from modelling using this boundary condition can be seen as quantitative when the carriers exhibit diode-behavior.

The fact that we use a single $J_{0\mathrm{x}}$ for each carrier implies that we are treating the interface as uniform. In partially crystalline semiconductors, it is possible that the interface is characterized by a collection of processes in parallel, each defined by their own $J_{0\mathrm{x}}$ value. This is part of the motivation for using a single crystal Si cell to explore the fundamental physics with less complication from the potential for heterogeneity as might be present in polycrystalline absorbers.

Several theories of semiconductor interfaces predict partial currents of the form of eqn (S1) including the Shockley pn junction model,[2] and the thermionic emission model applied to Schottky-like diodes[3] and in certain cases to heterojunctions.[4] These models are all applied to semiconductors with free electronic carriers so they do not apply to low dielectric absorbers, such as organic semiconductors, where excitons are formed.

The most relevant model for the work herein is the thermionic emission model.[5] The simplest application of thermionic emission is to treat charge transfer between a semiconductor and a good conductor that cannot support a depletion region, and we refer to this as the Schottky model. The classic example is the semiconductor/metal (Schottky) interface,[3] but the models is also widely applied to molecular contacts to semiconductors in particular in the area of semiconductor photoelectrochemistry.[6] In these cases, the J_0 is given by eqn (3) in the main text, reproduced here:

$$J_{0\mathrm{x}} = \kappa_{\mathrm{x}} A^{*}_{\mathrm{x}} T^{2} e^{\left(\frac{-q\phi_{\mathrm{bx}}}{kT}\right)} \qquad S2$$

Here, the $J_{0\mathrm{x}}$, ϕ_{b} and κ are the exchange current density, barrier height, and transmission coefficient with the *x* label indicating quantities for electrons (x=n) or holes (x=p). The ϕ_{bn} is given by the difference between the conduction band of the semiconductor and the Fermi level of the contact, and the ϕ_{bp} is given by the difference between the valence band of the semiconductor and the Fermi level of the contact (see Fig. S4a). The κ is the fraction of carriers incident on the immediate interface that actually cross, and it depends on the density of states in the contact at the energy of the relevant absorber band edge as shown schematically in Fig. S4a. For metals, which have a continuous and very high density of states, $\kappa_{\mathrm{x}} = 1$, but for molecular contacts, it can be orders of magnitude lower due to slow carrier transfer at the immediate semiconductor/metal interface as described by electron transfer models such as those of Gerischer.[7]

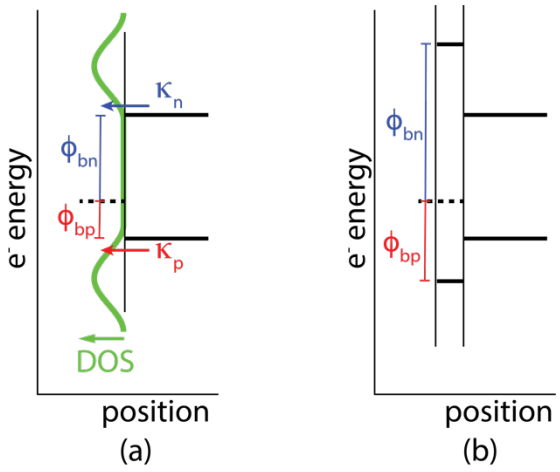

Fig S4 (a) Thermionic emission applied to a Schottky type interface with electron and hole barrier heights defined by the differences between the Fermi level of the contact and the band edges of the absorber and with the density of states (DOS) of the interfacial layer determining the κ values at the interface. (b) Thermionic emission model applied to a Type I heterojunction with the barrier heights given by the differences between the band edges of a larger band gap interfacial layer and the Fermi level of the contact.

We have intentionally used thin layers in this study to isolate sprio-OMeTAD's impacts on interfacial charge transfer from contributions of bulk transport. As such, we view the action of spiro-OMeTAD interfacial layers as a perturbation to a metal contact as would be described by eqn (S2). In this case, the spiro-OMeTAD can be seen to shift the Fermi level of the metal relative to the band edge positions thereby changing ϕ_{bn} and ϕ_{bp} in a way (one goes up and one goes down) that changes J_{0n}/J_{0p} but not $(J_{0n}J_{0p})^{0.5}$. The spiro-OMeTAD also results in a reduction in κ_n and κ_p due to a lower, more localized (in energy space) density of states relative to a metal. If κ_n and κ_p change to the same degree, the $(J_{0n}J_{0p})^{0.5}$ changes but J_{0n}/J_{0p} does not.

The spiro-OMeTAD layer could alternately be viewed as forming a heterojunction with transport described by thermionic emission of carriers between the two semiconductors making up the heterojunction. The heterojunction approach is often taken in modelling spiro-OMeTAD layers in perovskite solar cells and is necessary with thicker layers where bulk transport through the spiro-OMeTAD needs to be considered.[8] In the heterojunction case, eqn (S2) can still apply but with the meaning of ϕ_{bn} and ϕ_{bp} changed, and again in the thin layer limit. We have previously performed simulations of thin contact layers modelled as Type I heterojunctions using the standard heterojunction thermionic emission boundary conditions defined in COMSOL.[10] These simulations were in good agreement with a model of current-voltage behavior derived using the boundary condition of eqns (S1) and (S2) but with ϕ_{bn} and ϕ_{bn} defined as the difference between the Fermi level of the contact and the band edges of the contacting layer (not the absorber as in the Schottky model) as shown in Figure S4b. Here, the action of spiro-OMeTAD can be seen as altering the Fermi level of the contact and therefore shifting the band edge positions and ϕ_{bn} and ϕ_{bp} just as in the Schottky model. In this case, the larger band gap of the spiro-OMeTAD relative to the silicon absorber results in $\phi_{bn} + \phi_{bp}$ being higher than in the Schottky approach if it forms a Type I heterojunction. This effectively reduces the $(J_{0n}J_{0p})^{0.5}$ and has the same phenomenological effect as reducing κ in the Schottky model.

The boundary condition of eqns (S1) and (S2) can be applied in either the Schottky or heterojunction thermionic emission models. As our experiments directly measure J_0 rather than ϕ_{bn} or ϕ_{bp} we cannot distinguish between the two interpretations. Although we choose to interpret

changes in J_0 in the main text in terms of a perturbation to the semiconductor/metal interface and in terms of changes in κ, we also point out that these changes could be interpreted in terms of band edge offsets with the interfacial layer, *i.e.*, a heterojunction. With either model, the change in J_{0n}/J_{0p} can be seen as a work function effect raising one of ϕ_{bn} or ϕ_{bp} and lowering the other. Figure S5 shows the relative band edge positions of silicon and spiro-OMeTAD as isolated materials and the Fermi level of gold. There are two key features. First, the band gap of silicon is much smaller than that of spiro-OMeTAD, which provides a mechanism for increasing ϕ_{bn} or ϕ_{bp} from the metal limit in the heterojunction viewpoint. Second, their valence bands nearly align. We do not show a band diagram of the fully contacted system because the band edge offsets are expected to be different due to interactions between the materials. Further, our measurements do not distinguish band edge offsets from simple reduced densities of states relative to a metal, and hence do not provide the information necessary to construct a band diagram of the fully contacted system. Similarly, we do not show how these band edges might change when modified with spiro-OMeTAD. We instead rely on how the J_0 values change as fundamental measures of changes in the kinetics of electron *vs*. hole transfer, which is the focus of our work.

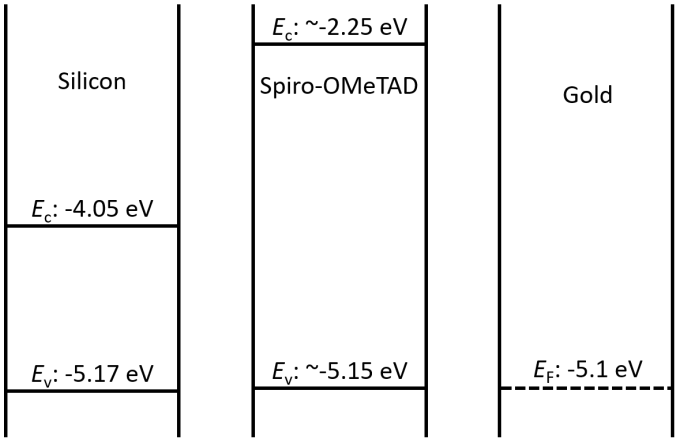

Fig S5 Conduction and valence band energies (E_C and E_V, respectively) of silicon and spiro-OMeTAD and Fermi level (E_F) of gold.

Deposition Solution Age Considerations

The IBC cell results for spiro-OMeTAD/Li-TFSI films depended on the age of the deposition solution. To illustrate, Fig. S6 shows a comparison of the J_0 results when "aged" vs. "fresh" solutions are used for interfacial fabrication. In this case, "fresh" means the solution was made directly before the film was spin coated while "aged" means the solution was kept nominally under nitrogen for 24 hours or more. Significant differences were not observed for solutions age beyond 24 hours. As shown in Fig. S6, the aging of the solution resulted in similar values of $(J_{0n}J_{0p})^{0.5}$ but increased values of J_{0p}/J_{0n} relative to fresh solutions. The trend with solution age is the same as with air exposure of the prepared films suggesting oxidation of spiro-OMeTAD by residual oxygen in the solutions.

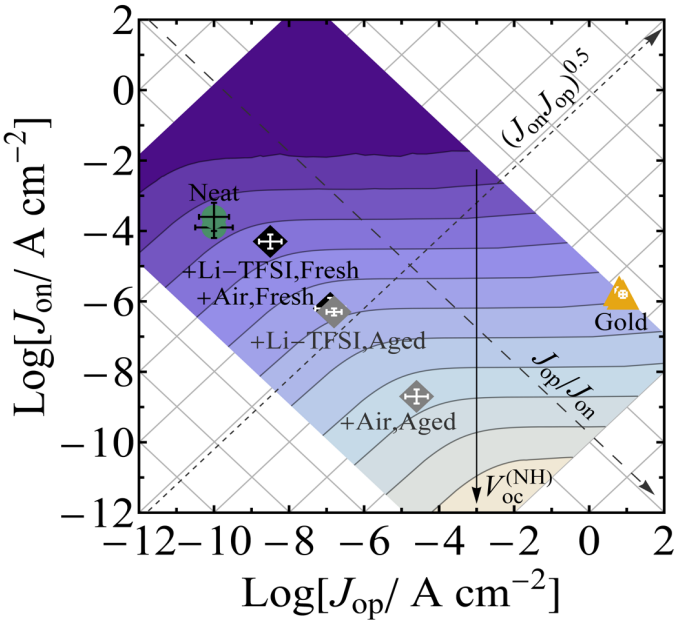

Fig S6 J_0 results comparing gold contacts modified with Li-TFSI-containing spiro-OMeTAD films made from "aged" vs. "fresh" solutions. The J_{0p}/J_{0n} is affected due to oxidation (*i.e.*, samples made with aged solutions are more oxidized to begin with than those made with fresh solutions), but solution age has little impact on $(J_{0n}J_{0p})^{0.5}$. The data for the aged samples is for three samples made from solutions that had been aged for at least 24 hours; the other data is the same as in Fig. 7 of the paper.

Relationships between carrier selectivity and current-voltage behavior

In general, the QFLS in a solar cell is determined by the balance of generation due to solar photons and recombination. In the case of contact-limited solar cells specifically, it is assumed that the QFLS will be limited by the balance of generation and contact recombination. One can exceed this level of QFLS only if one applies an external voltage that induces further "generation" by injecting additional carriers at the contacts, which is what happens when the applied voltage exceeds the V_{oc} of a solar cell. One can think of the QFLS as the maximum energy per carrier that can be extracted from a device. In order to support such a voltage (*i.e.*, in order for a device to operate in the power quadrant at such a voltage), sufficient asymmetry must also exist so that electrons are collected at one contact and holes at the other. This asymmetry can be quantified by the carrier selectivity.[9]

The theoretical relationship between carrier selectivity and the current-voltage ($J(V)$) behavior in a contact-limited solar cell has been discussed in some detail in Roe et al..[10] To briefly summarize, in a contact-limited device, the carrier selectivities determine the voltages at which the "steps" in the $J(V)$ curve occur. Each carrier governs a single step in the $J(V)$ curve so in general there are two steps that occur. However, the step that occurs at the lowest forward voltage – dictated by the limiting carrier selectivity – will always limit the device performance. This is because the minimum current of a single step is always enough to reverse the direction of current therefore removing the $J(V)$ curve from the power quadrant and determining V_{oc}. In other words, when the applied voltage, V, exceeds the smallest of the two carrier selectivities according to $V > V_T \ln(S_{car})$, the contacts can no longer support the photocurrent and the external circuit starts driving the current in the opposite direction. Here, V_T is the thermal voltage and S_{car} is the smaller of the two carrier selectivities. For a solar cell to *not* be limited by carrier selectivity, we require that the voltages associated with both carrier selectivities are larger than the maximum QFLS (in voltage units) that is able to be supported by the unavoidable recombination in the device. For a more complete picture of how the carrier densities at the contacts lead to the critical points on the $J(V)$ curve, see the supplementary material of Roe *et al*.[10]

Notes and References

1. T. Kirchartz, B.E. Pieters, K. Taretto, U. Rau, Mobility dependent efficiencies of organic bulk heterojunction solar cells: Surface recombination and charge transfer state distribution, *Phys. Rev. B*, 2009, **80**, 035334- 1-6.
2. Shockley, Bell System Technical Journal, 1949, **28,** 435-489.
3. E.H. Rhoderick and R.H. Williams, 1988, Metal-Semiconductor Contacts, Clarendon Press; Oxford University Press 1988.
4. K. Yang, J.R. East, G.I. Haddad, Numerical modelling of abrupt heterojunctions using a thermionic-field emission boundary condition, *Solid-State Electronics*, 1993, **36**, 321-330.
5. C. Herring, M.H. Nichols, Thermionic Emission, *Rev. Mod. Phys.*, 1949, **21**, 185-270.
6. M.X. Tan, P.E. Laibinis, S.T. Nguyen, J.M. Kesselman, C.E. Stanton, N.S. Lewis, 1994, Principles and Applications of Semiconductor Photoelectrochemistry, Progress in Inorganic Chemistry, John Wiley & Sons, Inc. 1994.
7. H. Gerischer, Electron-transfer kinetics of redox reactions at the semiconductor/electrolyte contact, *J. Phys. Chem.*, 1991, **95**, 1356-1359.
8. A. Alnuaimi, I. Almansouri, A. Nayfeh, Effect of mobility and band structure of hole transport layer in planar heterojunction perovskite solar cells using 2D TCAD simulation, *J. Comput. Electron.*, 2016, **15**, 1110-1118.
9. The essential difference between the V_{oc} and the QFLS can be exemplified by considering a semiconductor contacted on both sides by two identical, thick insulators. The QFLS in such a device could potentially be quite large, as the insulators are unlikely to allow for significant contact recombination. However, one could not measure a photovoltaic effect, or an appreciable V_{oc} from such a device, because there would not be enough asymmetry to give electrons and holes an energetic preference for one side of the device *vs.* the other.
10. E.T. Roe, K.E. Egelhofer, M.C. Lonergan, Exchange current density model for the contact-determined current-voltage behavior of solar cells, *J. Appl. Phys.*, 2019, **125**, 225302-1-12.